RSC Advances

PAPER

View Article Online
View Journal | View Issue

Cite this: *RSC Adv.*, 2022, **12**, 6328

Preparation of Ag_3PO_4/α-Fe_2O_3 hybrid powders and their visible light catalytic performances

Ya Gao,[a] Haodong Ma,[b] Chengliang Han,[b] Chengmei Gui *[bc] and Chonghai Deng[b]

Received 22nd December 2021
Accepted 8th February 2022

DOI: 10.1039/d1ra09256a

rsc.li/rsc-advances

The inefficiency of conventional photocatalytic treatment for removing rhodamine B is posing potential risks to ecological environments. Here, we construct a highly efficient photocatalyst consisting of Ag_3PO_4 and α-Fe_2O_3 hybrid powders for the treatment of rhodamine B. Ag_3PO_4 nanoparticles (nanoparticles, about 50 nm) are uniformly dispersed on the surface of α-Fe_2O_3 microcrystals (hexagonal sheet, about 1.5 μm). The Ag_3PO_4-deposited uniformity on the α-Fe_2O_3 surface first increased, then decreased on increasing the hybrid ratio of Ag_3PO_4 to α-Fe_2O_3. When the hybrid ratio of Ag_3PO_4 to α-Fe_2O_3 is 1 : 2, the distribution of Ag_3PO_4 particles on the sheet α-Fe_2O_3 is more uniform with excellent Ag_3PO_4/α-Fe_2O_3 interface performance. The catalytic degradation efficiency of hybrids with the introduction of Ag_3PO_4 nanoparticles on the α-Fe_2O_3 surface reached 95%. More importantly, the hybrid material exhibits superior photocatalytic stability. Ag_3PO_4/α-Fe_2O_3 hybrids have good reusability, and the photocatalytic efficiency could still reach 72% after four reuses. The excellent photocatalytic activity of the as-prepared hybrids can be attributed to the heterostructure between Ag_3PO_4 and α-Fe_2O_3, which can effectively inhibit the photoelectron–hole recombination and broaden the visible light response range.

1. Introduction

Due to its green, high efficiency, stability and environmental friendliness, photocatalytic wastewater treatment has become one of the most promising water treatment technologies.[1–4] Nano-TiO_2 photocatalyst is the most widely used catalyst.[5–8] However, the application of TiO_2 nanomaterials is limited due to their wide band gap ($E_g = \sim$2.4 eV), low quantum efficiency and low visible light utilization rate. It is well known that Ag_3PO_4 has a band gap of 2.36 eV and can absorb visible light and ultraviolet light with wavelengths less than 525 nm. The high quantum efficiency makes Ag_3PO_4 a potential visible light catalyst.[9–13] However, the high cost and poor stability of Ag_3PO_4 limit its large-scale application. The reduction of silver ions to silver on the surface can be effectively inhibited by semiconductor compositing, metal ion doping and introducing carbon materials, and a heterostructure can be formed to improve the stability and photocatalytic activity of Ag_3PO_4. Du *et al.*[14] successfully constructed novel Z-scheme Ag_3PO_4/g-C_3N_4 heterostructures with a high photocatalytic effect. The improved photocatalytic efficiency of Ag_3PO_4/g-C_3N_4 may be attributed to the formation of Z-scheme heterostructure structure and matching valence band and conduction band. Zhouyue Wu *et al.*[15] designed and synthesized hybrid AgI@Ag_3PO_4 nanostructures for visible-light photodegradation of norfloxacin *via* a facile self-assembly formation strategy. The experimental results indicated that the AgI@Ag_3PO_4-15 sample presented the best visible-light photocatalytic performance, which was far better than that of pristine AgI and 2.96 times that of pristine Ag_3PO_4. Hematite (α-Fe_2O_3) has a narrow band gap ($E_g \sim$ 2.2 eV) and a maximum absorption wavelength of about 560 nm. It has a high utilization rate of visible light such as sunlight. Moreover, α-Fe_2O_3 is a very promising visible light catalyst with low price, environmental protection and high stability, and has a good application prospect in the field of water treatment. It has become one of the hot topics of research in recent years.[16–19]

In this study, Ag_3PO_4/α-Fe_2O_3 hybrids were prepared by hydrothermal methods. Ag_3PO_4 nanoparticles were loaded on the hexagonal α-Fe_2O_3 sheets, which greatly improved the dispersion of Ag_3PO_4 nanoparticles and increased the specific surface area of hybrids. Thus, the visible light catalytic activity of Ag_3PO_4 will be further improved. The excellent photocatalytic activity of as-prepared hybrids can be attributed to the heterostructure between Ag_3PO_4 and α-Fe_2O_3, which can effectively inhibit the photoelectron–hole recombination and broaden the visible light response range.[20–23]

2. Experiment section

2.1 Preparation of Ag_3PO_4/α-Fe_2O_3 hybrids

Ag_3PO_4 nanopowder. 0.25 g $AgNO_3$ and a certain amount of polyvinylpyrrolidone were dissolved in 60 mL ionized water, and the solution A was obtained by ultrasonication for 5 min. 0.19 g

[a]*Center of Analysis and Testing, Hefei University, Hefei 230601, China*
[b]*School of Energy Materials and Chemical Engineering, Hefei University, Hefei 230601, China. E-mail: guichengmei@163.com*
[c]*School of Chemistry and Chemical Engineering, Chaohu University, Hefei 230009, China*

Na_2HPO_4 was dissolved in 60 mL ionic water and ultrasonicated for 5 min to obtain solution B. In dark, under 75 °C with continuous stirring, solution B was added to solution A drop by drop and then the solution was left in dark for 30 min. The product was centrifuged, washed twice with deionized water and ethanol, and dried at 60 °C in a vacuum to obtain Ag_3PO_4 powder, as show in Fig. 1.

α-Fe_2O_3 hexagonal sheets. 1.42 g $FeCl_3 \cdot 6H_2O$ and 2 g of NaOH were dissolved in 60 mL ionic water. The solution was transferred into a kettle for hydrothermal reaction at 180 °C for 24 h. After the reaction, the product was washed with deionized water to neutral, and α-Fe_2O_3 was obtained, as show in Fig. 1.

Ag_3PO_4/α-Fe_2O_3 hybrids. 0.156 g α-Fe_2O_3 and a certain amount of polyvinylpyrrolidone were ultrasonically dispersed in 60 mL of water, and then a certain amount of Ag_3PO_4 was added to form the precursor solution. The precursor was placed in the reactor for hydrothermal reaction at 160 °C for 10 h. The reactor was then cooled to room temperature and the product was washed twice, first with deionized water then ethanol, hence obtaining the Ag_3PO_4/α-Fe_2O_3 hybrid. The hybrids with molar ratios of 1 : 4, 1 : 3, 1 : 2 and 1 : 1 of Ag_3PO_4 to α-Fe_2O_3 were also prepared, as shown in Fig. 1.

2.2 Photocatalytic experiments

First, 50 mg Ag_3PO_4/α-Fe_2O_3 hybrid powder was ultrasonically dispersed in 100 mL rhodamine B solution with a concentration of 5 mg L^{-1}. Then, the solution was magnetically stirred for 30 min in a darkroom to enable the catalyst and dye reach the equilibrium of adsorption and desorption. The photocatalytic performance was tested using a xenon lamp as the light source to simulate sunlight. 4 mL of the solution was taken every 5 min, and the absorbance of the solution was measured by UV-Vis spectrophotometer after centrifugation.

3. Results and discussions

The crystal phase of pure Ag_3PO_4, α-Fe_2O_3 and the Ag_3PO_4/α-Fe_2O_3 hybrid (1 : 2) was confirmed by XRD, as shown in Fig. 2.

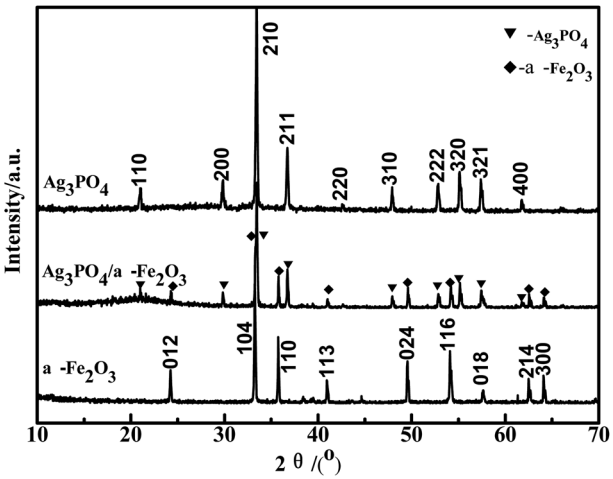

Fig. 2 XRD patterns of Ag_3PO_4, α-Fe_2O_3 and Ag_3PO_4/α-Fe_2O_3 hybrid.

The characteristic peaks of Ag_3PO_4 in Fig. 2 correspond to PDF# 06-0505, which is the cubic phase silver phosphor. Diffraction peaks at 20.83°, 29.64°, 33.25°, 36.53°, 47.75°, 52.65°, 54.97°, 57.24° and 61.60° correspond to (110), (200), (210), (211), (310), (222), (320), (321), (400) crystal surfaces.[24] The diffraction peaks at 24.14°, 33.15°, 35.61°, 49.48°, 54.09°, 62.45°, 63.99° correspond to the hexagonal α-Fe_2O_3 (012), (104), (110), (024), (116), (214), (300) crystal planes.[25] The characteristic peaks of Ag_3PO_4 and α-Fe_2O_3 can be clearly observed in the XRD spectra of the Ag_3PO_4/α-Fe_2O_3 hybrid, which indicates that Ag_3PO_4 and α-Fe_2O_3 are successfully combined with each other. In addition, no diffraction peaks of other impurities were found on the XRD patterns, indicating that the samples had high purity. The XRD characteristic peaks of the hybrids did not change, indicating that the hybrid had no obvious effect on the crystal structure.

The morphology and structure of the catalyst can significantly affect its catalytic performance. The morphology and composition of the Ag_3PO_4/α-Fe_2O_3 hybrid photocatalyst were characterized by scanning electron microscopy (SEM) and energy dispersive spectroscopy (EDS). Fig. 3 shows the SEM

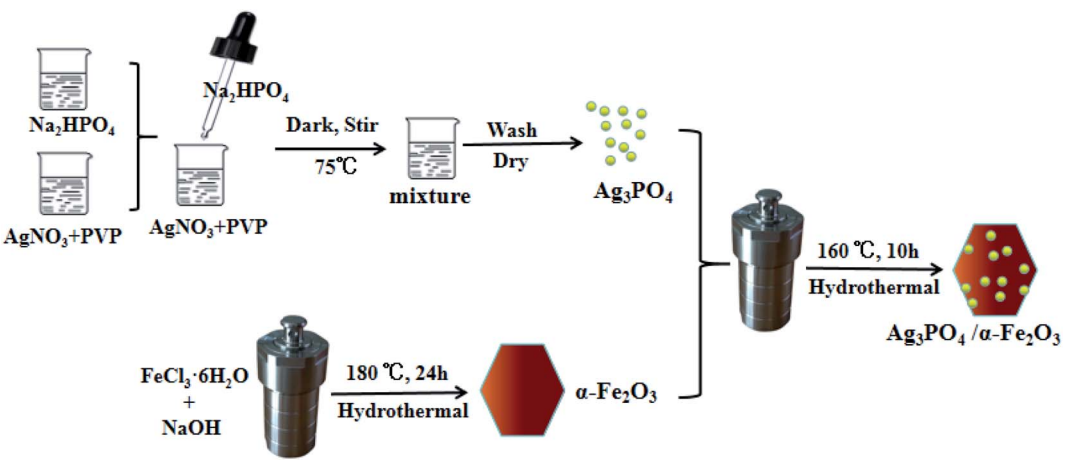

Fig. 1 Flow chart of Ag_3PO_4/α-Fe_2O_3 preparation.

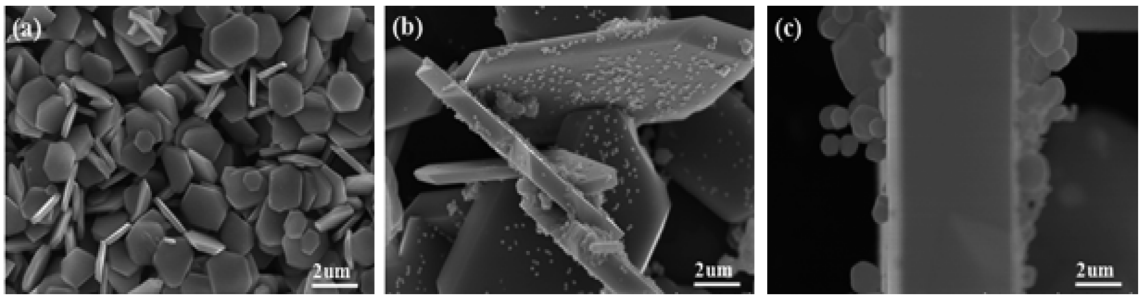

Fig. 3 SEM images of α-Fe_2O_3 and Ag_3PO_4/α-Fe_2O_3 hybrid (a–c).

images of pure α-Fe_2O_3 and Ag_3PO_4/α-Fe_2O_3 hybrid (1 : 2). Fig. 3(a) shows α-Fe_2O_3 is a uniform hexagonal sheet structure with a size of about 1.5 μm. In Fig. 3(b), the SEM images manifests that the small Ag_3PO_4 particles deposited on the α-Fe_2O_3 sheet surface, with sizes of about 50 nm. From the side view of Ag_3PO_4/α-Fe_2O_3 in Fig. 3(c), it can be seen that Ag_3PO_4 nanoparticles are closely bonded with α-Fe_2O_3 sheets, which is conducive to the migration of photoelectric charge carriers between them to form a hybrid catalyst with high catalytic activity.[26]

Fig. 4 shows the SEM photos of Ag_3PO_4/α-Fe_2O_3 hybrids with different proportions. It can be clearly seen from Fig. 4 that with the increase in the hybrid ratio of Ag_3PO_4 and α-Fe_2O_3, the deposited uniformity of Ag_3PO_4 particles on α-Fe_2O_3 surface first increased, and then decreased. When the hybrid ratio of Ag_3PO_4 and α-Fe_2O_3 is 1 : 2, the distribution of Ag_3PO_4 particles on the sheet α-Fe_2O_3 is more uniform and dispersed. In addition, the Ag_3PO_4/α-Fe_2O_3 hybrid exhibited excellent interface performance.

Fig. 5 demonstrates the EDS scan analysis spectrum of each Ag_3PO_4/α-Fe_2O_3 hybrid photocatalyst element. It can be seen from Fig. 5(a) that the small particles protruding from the sheet structure mainly contain Ag, P, O elements, and the sheet structure is mainly composed of Fe and O elements. According to the line scanning analysis figure, the small particles on the α-Fe_2O_3 sheet structure are Ag_3PO_4 particles, which further proves that the Ag_3PO_4/α-Fe_2O_3 hybrid photocatalyst has been successfully prepared. Fig. 5(b) shows that O, Fe, P, and Ag elements exist in the hybrid, and from the AT% of Ag/Fe = 3.09/4.26 = 0.73 ≈ 0.75 (= 3/4), it can be roughly inferred that the mole ratio of Ag_3PO_4 and α-Fe_2O_3 is 1 : 2. Because EDS results are affected by test location, only semi-quantitative analysis can be carried out.

The light absorption properties of Ag_3PO_4, α-Fe_2O_3 and Ag_3PO_4/α-Fe_2O_3 hybrids were analyzed by UV-Vis diffuse

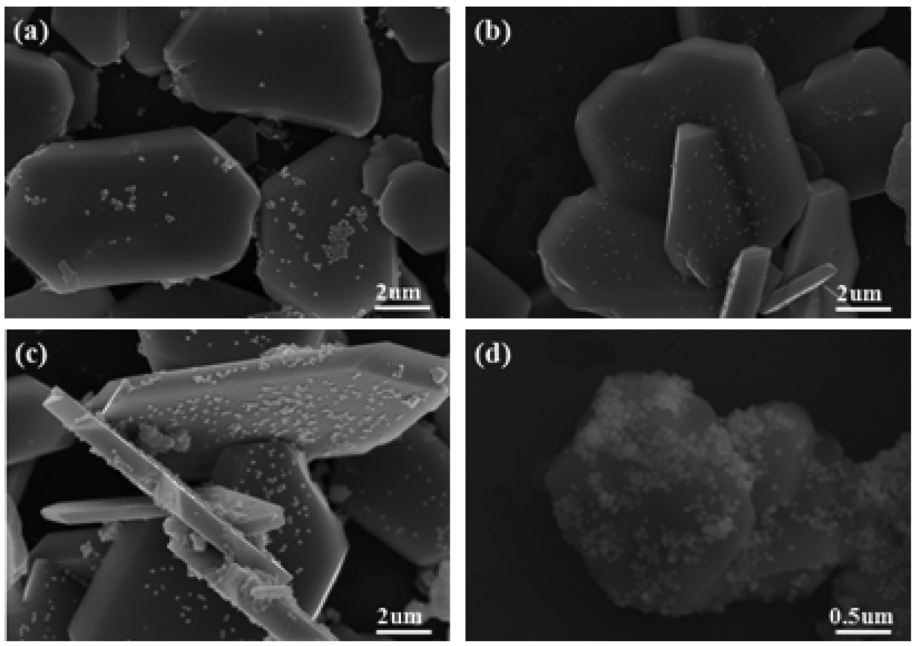

Fig. 4 SEM photographs of Ag_3PO_4/α-Fe_2O_3 hybrids with different proportions, the ratios of Ag_3PO_4 and α-Fe_2O_3 are: (a)1 : 4; (b) 1 : 3; (c) 1 : 2; (d) 1 : 1.

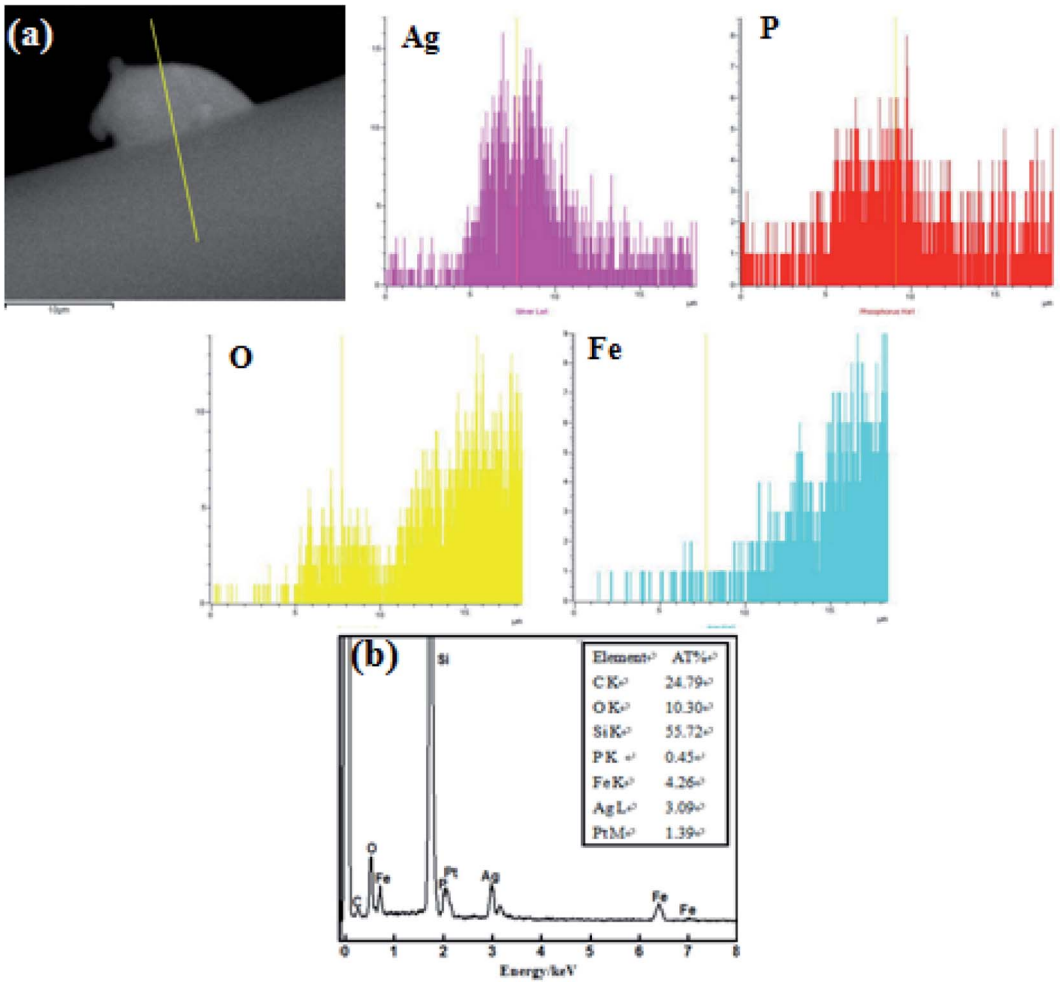

Fig. 5 EDS line scanning across the Ag_3PO_4/α-Fe_2O_3 hybrid (a) and its EDS spectrum (b).

reflectance spectroscopy. Fig. 6(a) shows the UV-Vis diffuse reflectance absorption spectra of pure Ag_3PO_4, α-Fe_2O_3 and Ag_3PO_4/α-Fe_2O_3 complex (1 : 2). It can be seen from Fig. 6(a) that the maximum light absorption band edges of pure Ag_3PO_4 and α-Fe_2O_3 are about 550 nm and 650 nm, respectively. Compared with pure Ag_3PO_4, the absorption wavelength of the Ag_3PO_4/α-Fe_2O_3 hybrid photocatalyst in the visible light region has a red shift, which enhances the visible

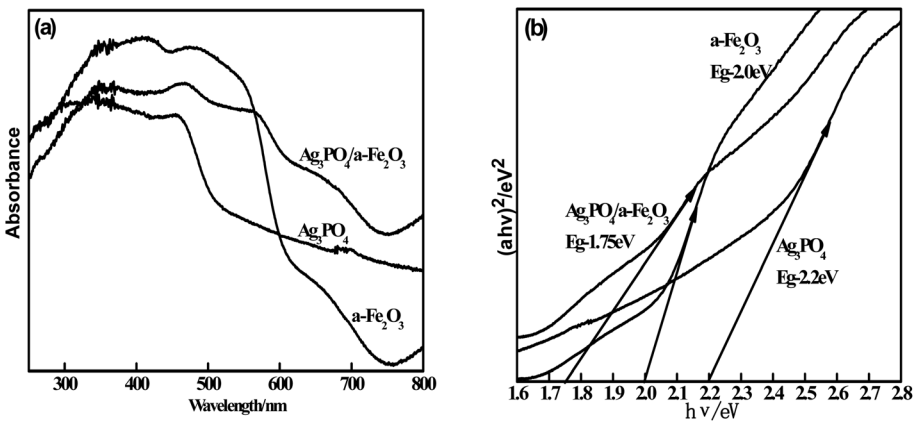

Fig. 6 UV-Vis spectra (a) and the corresponding $(\alpha h\nu)^2$–$h\nu$ curve of the Ag_3PO_4, α-Fe_2O_3 and Ag_3PO_4/α-Fe_2O_3 hybrid(b).

light response range thus increasing the utilization rate of light. The red-shift phenomenon is attributed to the heterojunction structure formed between Ag_3PO_4 and α-Fe_2O_3 which may be induced by the structural defects, and the enhanced internal stress results in the overlap of the electron wave function generated in the process. From the $(\alpha h\nu)^2 \sim h\nu$ curve in Fig. 6(b), it can be concluded that the E_g values of Ag_3PO_4 and α-Fe_2O_3 are about 2.2 eV and 2.0 eV, respectively.[27,28] The valence band E_{VB} and conduction band position E_{CB} can be obtained from the calculation formula of the semiconductor energy band structure:[29]

$$E_{VB} = X - E^e + 0.5E_g \quad (1)$$

$$E_{CB} = E_{VB} - E_g \quad (2)$$

X is the absolute electronegativity of the semiconductor, and the X values of Ag_3PO_4 and α-Fe_2O_3 are 6.20 eV and 5.87 eV, respectively; E^e is the energy of a free electron on the hydrogen scale (about 4.5 eV). Therefore, the E_{VB} and E_{CB} of Ag_3PO_4 are 2.80 eV and 0.60 eV, and the E_{VB} and E_{CB} of α-Fe_2O_3 are 2.37 eV and 0.37 eV, respectively.

The photocatalytic activity of Ag_3PO_4, α-Fe_2O_3 and Ag_3PO_4/α-Fe_2O_3 hybrid photocatalyst for rhodamine B degradation under visible light was investigated. It can be seen from Fig. 7(a) that rhodamine B hardly degrades itself. At the same time, the degradation efficiency of pure Ag_3PO_4 and α-Fe_2O_3 for rhodamine B was 82% and 8%, respectively, after 10 min of visible light catalysis. It can be clearly seen from Fig. 7(b) that, compared with pure α-Fe_2O_3, the photocatalytic degradation effect of rhodamine B by loading Ag_3PO_4 on α-Fe_2O_3 has been greatly improved. With the increase in the Ag_3PO_4 load, the catalytic activity of the Ag_3PO_4/α-Fe_2O_3 hybrid photocatalyst first increased and then decreased. When the molar ratio of Ag_3PO_4 to α-Fe_2O_3 was 1 : 2, the catalytic degradation ability of rhodamine B solution was the best, and the catalytic degradation efficiency reached 95% after 10 min. Combined with the SEM images of Ag_3PO_4/α-Fe_2O_3 hybrids with different ratios shown in Fig. 4, it can be predicted that when the composite ratios of Ag_3PO_4 and α-Fe_2O_3 are 1 : 4 and 1 : 3, fewer Ag_3PO_4 particles are loaded on the sheet α-Fe_2O_3, which is unfavorable to the migration of photoelectric charge carriers between the two and hence unfavorable to the improvement of photocatalytic activity. When the composite ratio of Ag_3PO_4 and α-Fe_2O_3 is 1 : 2, the distribution of Ag_3PO_4 particles on the sheet α-Fe_2O_3 is more uniform, which improves the dispersion of Ag_3PO_4 particles and increases the photocatalytic specific surface area. The heterojunction structure formed between Ag_3PO_4 and α-Fe_2O_3 effectively promoted the separation of photogenerated electrons and holes and improved the electron migration efficiency, thus improving the photocatalytic activity of the material.[30,31] However, too much Ag_3PO_4 will cause Ag_3PO_4 particles to agglomerate on the sheet α-Fe_2O_3, which will reduce the surface activity of Ag_3PO_4/α-Fe_2O_3, thus reducing the photocatalytic activity of the composite photocatalyst. At the same time, it can be seen that the catalytic activity of the Ag_3PO_4/α-Fe_2O_3 hybrid photocatalyst is higher

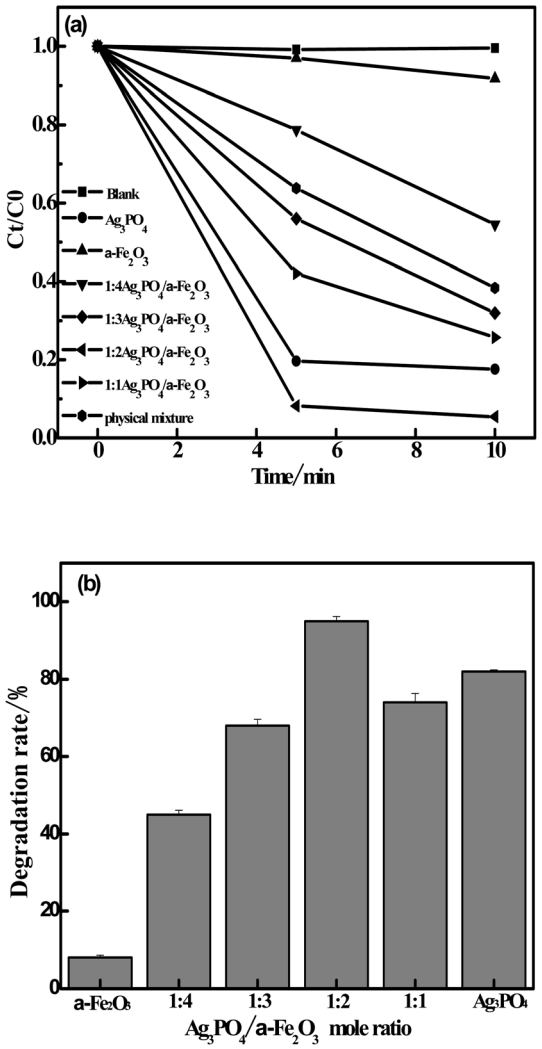

Fig. 7 Kinetic curves of degradation of rhodamine B (a); photocatalytic degradation curves of RhB solution by different catalyst samples (b).

than that of the physical mixture with the same proportion, which further indicates that the Ag_3PO_4/α-Fe_2O_3 hybrid photocatalyst prepared in this experiment formed a heterojunction structure and improved the photocatalytic activity, while the simple physical mixture cannot form a heterojunction structure.

The possible mechanism of the photocatalytic degradation of rhodamine B by the Ag_3PO_4/α-Fe_2O_3 hybrid photocatalyst is shown in Fig. 8. Under simulated solar irradiation, because the gap width of Ag_3PO_4 and α-Fe_2O_3 is narrow, and the absorbability is good in the range of visible wavelength, the electrons in the valence band are easily excited to transition to the conduction band, while the holes remain in the valence band. First, the E_{CB} (0.60 eV) of Ag_3PO_4 is higher than that of α-Fe_2O_3 (0.37 eV), and the photogenerated electrons in the α-Fe_2O_3 conduction band can easily migrate to the Ag_3PO_4 conduction band. The E_{VB} of Ag_3PO_4 (2.80 eV) is higher than that of α-Fe_2O_3 (2.37 eV), and the valence band holes of Ag_3PO_4 are transferred to the valence band of α-Fe_2O_3; thus, the photogenerated

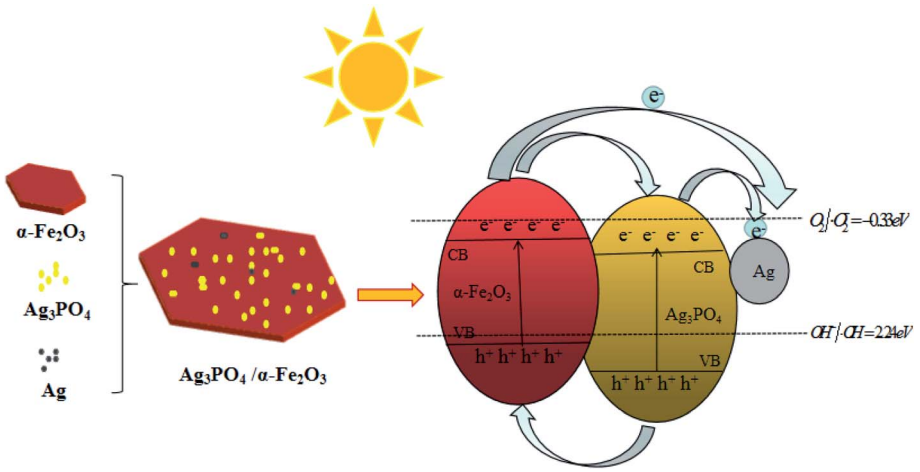

Fig. 8 Mechanism of enhanced photocatalytic activity.

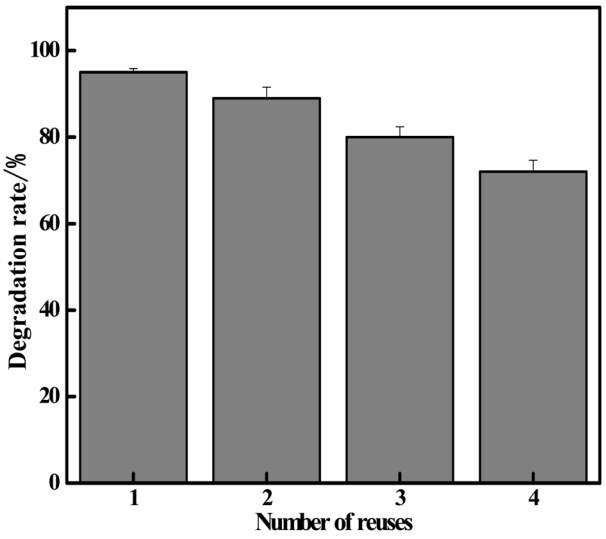

Fig. 9 Effect of reuse times of the Ag_3PO_4/α-Fe_2O_3 hybrid catalyst on RhB degradation rate.

electron–hole pair is effectively separated. Second, Ag_3PO_4 will produce a small amount of Ag due to the photocorrosion phenomenon, which can further capture electrons from the conduction band of Ag_3PO_4 and α-Fe_2O_3, thus promoting the separation of photogenerated electrons and holes, and enhancing the photocatalytic activity.

Fig. 9 shows the effect of repeated usage times of the Ag_3PO_4/α-Fe_2O_3 hybrid catalyst on the degradation rate of rhodamine B. It can be seen from Fig. 9 that the photocatalytic degradation rate of rhodamine B decreased from 95% to 72% after repeated use of the Ag_3PO_4/α-Fe_2O_3 hybrid catalyst for four times. The photocatalytic degradation rate decreased slightly, but the photocatalyst still had certain stability and could be reused many times. According to the XRD comparison patterns of the Ag_3PO_4/α-Fe_2O_3 hybrid catalyst before and after use in Fig. 10, it can be clearly seen that the main reason for the decrease in the catalytic degradation rate is that a small amount of elemental silver (Ag) is produced by the photocorrosion of Ag_3PO_4 during the degradation process.[32] Meanwhile, the loss of some amount catalyst in the processes of washing and recycling is also a reason for the reduction in the degradation rate.

Fig. 11 shows the UV-Vis absorption spectra of the Ag_3PO_4/α-Fe_2O_3 photocatalytic degradation of rhodamine B. It can be seen from Fig. 11 that with the extension of the photocatalytic degradation time, the absorption peak intensity of rhodamine B solution gradually decreased, and rhodamine B was almost completely degraded after 10 min. In the whole process of photocatalytic degradation, the position and shape of the absorption peak of rhodamine B did not change, and no new absorption peak was generated, indicating that the concentration of rhodamine B only decreased in the degradation process, and no new substances were generated. Finally, it was concluded that rhodamine B might be catalyzed to degrade to H_2O and CO_2.

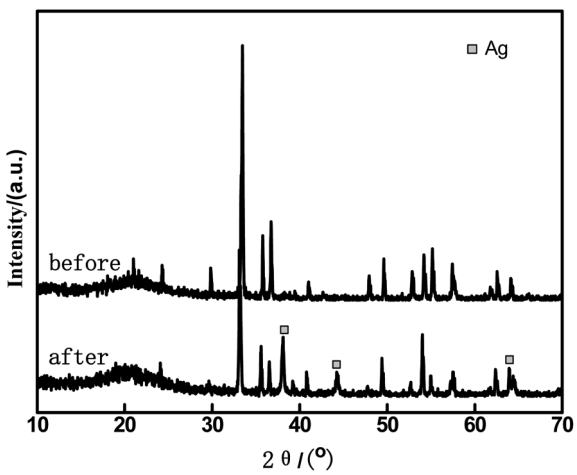

Fig. 10 XRD patterns of the Ag_3PO_4/α-Fe_2O_3 hybrid catalyst before and after application.

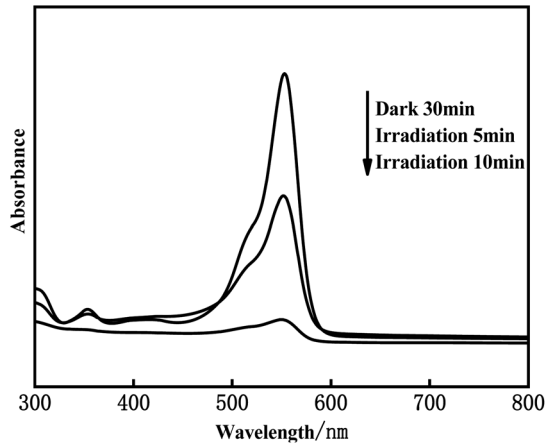

Fig. 11 UV-Vis spectra of Ag_3PO_4/α-Fe_2O_3 photocatalytic degradation of rhodamine B.

4. Conclusion

Based on a series of experiments and characterization, the following conclusions are drawn: when the molar ratio of Ag_3PO_4 to α-Fe_2O_3 is 1 : 2, the catalytic degradation of the rhodamine B solution was the highest, and the catalytic degradation efficiency reached 95% in 10 min, which was significantly higher than that of pure Ag_3PO_4 and α-Fe_2O_3. This may be because the small Ag_3PO_4 particles are uniformly dispersed on the α-Fe_2O_3 sheet structure, which increases the catalytic specific surface area of Ag_3PO_4 particles. Moreover, Ag_3PO_4 particles and α-Fe_2O_3 sheets were closely combined to form a heterojunction structure, which improved the migration of photogenerated electrons and holes between the two. Thus, the photocatalytic activity of Ag_3PO_4/α-Fe_2O_3 hybrids was improved. The Ag_3PO_4/α-Fe_2O_3 hybrids had good visible light catalytic activity and stability, and could be reused many times.

Author contributions

Y. Gao and C. M. Gui contributed to the conception and design of the work. H. D Ma, L. C. Han planned and designed the experiments, and made data acquisition. C. M. Gui, Y. Gao, H. D Ma, L. C. Han and H. C. Deng contributed to the analysis, data interpretation characterizing the samples. All authors have reviewed and approved to the final version of the manuscript.

Conflicts of interest

The authors declare that they have no known competing financial interests or personal relationships that could have appeared to influence the work reported in this paper.

Acknowledgements

This work was supported by Key Research and Development Program of Anhui Province (Grant No. 2019B11020040) and Natural Science Foundation of Anhui Province (Grant No. 1808085MB40) and National College Students Innovation Project (Grant No. 202111059024).

References

1 Q. Li, T. Shi, X. Li, K. G. Lu, M. Li, F. L. Liu, H. G. Li and M. Lei, *Appl. Catal., B*, 2018, **229**, 8.
2 J. J. Huang, W. P. Wu, R. X. Zhang, G. Q. Lu, B. Chen, Z. M. Chen and C. M. Gui, *Nano Energy*, 2002, **92**, 106734.
3 R. C. Shen, C. J. Jiang, Q. J. Xiang, J. Xie and X. Li, *Appl. Surf. Sci.*, 2019, **471**, 43.
4 J. J. Huang, L. L. Xu, D. F. Zhao, J. Wang, C. R. Chu, H. D. Chen, Y. H. Liu and Z. M. Che, *Chem. Eng. J.*, 2020, **383**, 123199.
5 M. J. Nalbandian, M. Zhang, J. Sanchez, S. Kim, Y.-H. Choa, D. M. Cwiertny and N. V. Myung, *J. Hazard. Mater.*, 2015, **299**, 141.
6 L. Cui, S. L. Liu, F. K. Wang, J. Y. Li, Y. H. Song, Y. Sheng and H. F. Zou, *J. Alloys Compd.*, 2020, **826**, 154001.
7 J. Singh, S. A. Khan, J. Shah, R. K. Kotnala and S. Mohapatra, *Appl. Surf. Sci.*, 2017, **422**, 953.
8 R. K. Nainani and P. Thakur, *Water Sci. Technol.*, 2016, **73**, 1927.
9 Y. Lyu, F. Wei, T. Zhang, L. Luo, Y. Pan, X. Yang, H. Yu and S. Zhou, *J. Alloys Compd.*, 2021, **876**, 160016.
10 Y. J. Lee, J. K. Kang, S. J. Park, C. G. Lee, J. K. Moon and P. J. J. Alvarez, *Chem. Eng. J.*, 2020, **402**, 126183.
11 Y. Ma, J. Li, Y. Jin, K. Gao, H. Cai and G. Ou, *Chemosphere*, 2021, **285**, 131440.
12 Z. Hu, J. Lyu and M. Ge, *Mater. Sci. Semicond. Process.*, 2020, **105**, 104731.
13 J. Wang, X. Yu, X. Fu, Y. Zhu and Y. Zhang, *Mater. Sci. Semicond. Process.*, 2021, **121**, 105329.
14 J. G. Du, Z. Xu, H. Li, H. J. Yang, S. J. Xu, J. Wang, Y. A. Jia, S. L. Ma and S. H. Zhan, *Appl. Surf. Sci.*, 2021, **541**, 148487.
15 Z. Y. Wu, J. P. Yu, W. F. Wang, C. H. X. H. Xin, X. Yu and Y. T. Tang, *J. Alloy. Compd.*, 2021, **891**, 161877.
16 Z. Jiang, W. Wan, H. Li, S. Yuan, H. Zhao and P. K. Wong, *Adv. Mater.*, 2018, **30**, 1706108.
17 Y. Geng, D. Chen, N. Li, Q. Xu, H. Li, J. He and J. Lu, *Appl. Catal., B*, 2021, **280**, 119409.
18 W. Wang, W. Zhao, H. Zhang, X. Dou and H. Shi, *Chin. J. Catal.*, 2021, **42**(1), 97.
19 P. Wu, X. Zhao, C. Li, M. Yang, G. Li, S. Zhang, J. Ming, M. Liu, Z. Qian and P. Fang, *New J. Chem.*, 2020, **44**, 16370.
20 W. Su, X. Liu, L. Tan, Z. Cui, Y. Liang, Z. Li, S. Zhu and S. Wu, *ACS Sustain. Chem. Eng.*, 2020, **8**, 2577.
21 M. Liu, X. Xue, S. Yu, X. Wang, X. Hu, H. Tian, H. Chen and W. Zheng, *Sci. Rep.*, 2017, **7**, 3637.
22 J. Xu, X. Li, J. Niu, M. Chen, J. Yue and J. Alloy, *Compd*, 2020, **834**, 155061.
23 P. F. Wang, P. H. Shi, Y. C. Hong, X. J. Zhou and W. F. Yao, *Mater. Res. Bull.*, 2015, **62**, 24.
24 L. Luo, Y. Li, J. Hou and Y. Yang, *Appl. Surf. Sci.*, 2014, **319**, 332.
25 P. Shao, Z. Ren, J. Tian, S. Gao, X. Luo, W. Shi, B. Yan, J. Li and F. Cui, *Chem. Eng. J.*, 2017, **323**, 64.

26 V. G. Deshmane, S. L. Owen, R. Y. Abrokwah and D. Kuila, *J. Mol. Catal. A: Chem.*, 2015, **408**, 202.
27 M. Q. Wen, T. Xiong, Z. G. Zang, W. Wei, X. T. Tang and F. Dong, *Opt. Express*, 2016, **24**, 10205.
28 D. Y. Liang, C. Cui, H. H. Hu, Y. P. Wang, S. Xu, B. L. Ying, P. G. Li, B. Q. Lu and H. L. Shen, *J. Alloys Compd.*, 2014, **582**, 236.
29 M. Wang, P. Y. Guo and G. J. Yang, *Mater. Lett.*, 2017, **192**, 96.
30 P. Kang, L. Zhang, B. Cheng and J. Yu, *Appl. Catal., B*, 2017, **218**, 570.
31 A. Liu, C. Zhang, Y. Zhu, K. Li, J. Huang, Y. K. Du and P. Yang, *J. Colloid Interface Sci.*, 2019, **535**, 408.
32 M. Ge, N. Zhu and N. Y. P. Zhao, *Ind. Eng. Chem. Res.*, 2012, **51**, 5167.